Optical Materials 121 (2021) 111629

Contents lists available at ScienceDirect

Optical Materials

journal homepage: www.elsevier.com/locate/optmat

Research Article

Shape-diversified silver nanostructures on Al foil fabricated in micellar template for high performance surface enhanced Raman scattering applications

Ying Zhang [a,*], Lishuang Yao [c], Lixiang Liu [a], Zenghui Peng [b], Zepeng Li [a], Hao Wang [a], Qingjun Zhou [a], Tong Wei [a], Yanrui Guo [a], Xiong Yang [a], Li Xuan [b]

[a] College of Science, Civil Aviation University of China, Tianjin, 300300, China
[b] State Key Laboratory of Applied Optics, Changchun Institute of Optics, Fine Mechanics and Physics, Chinese Academy of Sciences, Changchun, Jilin, 130033, China
[c] College of Science, Shantou University, Shantou, 515063, China

ARTICLE INFO

Keywords:
Surface enhanced Raman scattering
Silver nanoparticles on Al foil
Micellar template
Galvanic replacement reaction

ABSTRACT

Highly effective surface-enhanced Raman substrates with shape-diversified silver nanostructures on Al foil (AlF) were fabricated by galvanic replacement reaction in micellar template which is easy to control, simple and cost-effective. Due to the localized surface plasmon resonance (LSPR) of silver nanostructures, the substrates were used as surface enhanced Raman substrates. The shape-diversified silver nanostructures on AlF exhibited stronger surface enhanced Raman scattering (SERS) effects compared with flowerlike Ag nanostructures on ITO glass substrate fabricated by electrodeposition in micellar template. The maximum Raman enhancement factor of 10^9 fold was obtained, which is 236 times larger than the flowerlike silver nanostructures on ITO glass substrate. The scanning electron microscope (SEM) images show that the size and shape of the nanostructures and surface morphology make a valuable contribution to SERS. Raman enhancement experiments of three Raman probes were studied, which shows that different vibrational modes of Raman probe affect SERS effect. The fabricated shape-diversified silver nanostructures on AlF fabricated by galvanic replacement reaction in micellar template are cheap, controllable and simple. It could be potentially useful in SERS field such as imaging applications and highly sensitive molecule detecting.

1. Introduction

Nowadays, people are paying more and more attention to environmental pollution, disease, food safety and security. Sensitive and convenient detection methods have attracted many researchers' attention. Surface enhanced Raman scattering (SERS) as a technique for enhancing the Raman scattering intensity rapidly becomes a potential method for applications in fundamental and applied research such as food safety [1–6], forensic science [7], biotechnology [8,9] and sensing [10–12] due to its highly effective and label-free capability [13]. As we know, the SERS substrate plays a decisive role in the intensity enhancement of Raman signal. In SERS, one of the aims of the research is searching for substrates with properties of high-performance enhancement factor (EF), fabrication simplicity, cost-effective and controllability. Plenty of substrates such as noble metal based substrate and semiconductor based substrate have been studied and used in practical applications [14–16]. Noble metal based substrates which can provide an extremely strong electromagnetic field on the surface due to the excitation of surface plasmon have shown superior SERS effect [17]. Among noble metals, Ag stands out owing to its superior SERS effect derive from electrons in Ag which are sensitive to the electric field originated by the localized surface plasmon resonance (LSPR). Ag-based SERS substrates can be fabricated in many methods, for instance, chemical synthesis [18], chemical vapor deposition [19,20], electrochemical deposition [21,22], nano-lithography [23,24]. Plenty kinds of shapes and morphologies, such as nanoparticles [25,26], nanoplates [26], nanoprisms [27,28] and nanoclusters [29] have been studied as SERS substrates. Study shows that silver nanostructures with multi 'hotspots' (tips, gaps and corners) used as SERS substrates exhibit more favorable properties such as high enhancement factor. The redistribution of optical fields around the particle owing to rough surface-induced field superposition plays an important role in the high enhancement

* Corresponding author.
E-mail address: zhang_y@cauc.edu.cn (Y. Zhang).

https://doi.org/10.1016/j.optmat.2021.111629
Received 19 June 2021; Received in revised form 21 September 2021; Accepted 25 September 2021
Available online 5 October 2021

effect of metal particles [30]. Various kinds of substrates such as rosettelike nanocrystals [18], flowerlike nanostructures [31], dendrite nanostructures [32], nanoclusters [29] were investigated. In order to ensure the stability of the SERS substrates and convenience in the spectra measurement process, these nanostructures can also be placed or deposited onto a solid substrate such as glass [33,34]. However, reflectivity of glass is very low which is bad for SERS effect. In 2010, A. Gutés et al. firstly proposed silver nanostructures on aluminum foils obtained by galvanic displacement could be used as SERS substrates [32]. Aluminum as a metal with a high reflectivity can let the Raman scattering light return to Raman probe more efficiently. Besides, the optical phenomena caused by the coupling between the localized surface plasmon of nanostructure and the delocalized surface plasmon polariton from Al film benefits SERS effect [32,35–37]. Given the aforementioned reasons, silver nanostructures with multi hotspots on AlF have emerged as an excellent candidate for SERS substrate. However, there are still some problems with the fabrication such as complex production process, high cost, time consuming, poor reproducibility and so on, which limit the practical applications for the substrates. The metal nanostructure substrates still need to be studied. In this work, we investigated shape-diversified silver nanostructures on AlF for SERS applications by galvanic replacement reaction in micellar template which is cost-effective, simple and with improved SERS effect. Nanostructures with different shapes were obtained for different reaction times. Flowerlike silver nanostructures on ITO glass substrate and polished AlF were fabricated, measured and analyzed data as two control substrates for SERS. The enhancement factor of 10^9 was achieved by the shape-diversified silver nanostructures on AlF which is larger than the flowerlike silver nanostructures on ITO glass substrate and polished AlF. Reasons for the changes of EFs with different shape nanostructures were studied. Such shape-diversified silver nanostructures on AlF fabricated by galvanic replacement reaction in micellar template are of potential applications in SERS field.

2. Experimental

2.1. Materials

Anionic surfactant sodium bis (2-ethylhexyl) sulfosuccinate (AOT) (98 wt %), silver nitrate (99 wt %) and oil phase p-xylene (99 wt %) were obtained from Sigma-Aldrich Chemical Company. Deionized water whose resistivity is over 18MΩ·cm was obtained from the Millipore Elixir 100. Silver foil (2.0 mm 99%), Al foils (10.0 μm) and melamine were purchased from Alfa Aesar. Rhodamine 6G (R6G) was bought from J&K(China). 4-mercaptobenzoic acid (4-MBA) was bought from Macklin.

2.2. Fabrication of silver nanostructures

2.2.1. Preparation of Ag nanostructures on AlFs

The silver nanostructures on AlFs were fabricated in micellar template by galvanic replacement reaction. The AlFs were polished with finer-grade sandpaper (5000 meshes) to remove the oxide layer on the surface of the AlFs (10.0 μm Alfa Aesar) followed by a wash in ethanol (99.9 wt%). Process of synthesizing micellar template is the same as that described in our reports forehead [38]. The micellar template consists of the oil phase p-xylene, surfactant anionic surfactant sodium bis (2-ethylhexyl) sulfosuccinate (AOT) and $AgNO_3$ aqueous solution which replaced water in this work. Firstly, the AOT p-xylene solution with 1.4 M concentration was prepared. Then, $AgNO_3$ aqueous solution with 0.3 M was added to the AOT p-xylene solution drop by drop. After violent stirring for 2 h, the clear liquid mixture was used as micellar template and reducer in galvanic replacement reaction process. In the galvanic replacement reaction process, the polished AlFs were immersed in the micellar template prepared as mentioned above for different times at room temperature. The process was finished by taking the Ag nanostructures on AlF out of the micellar template. The Ag nanostructures on AlF substrates were washed gently by ethanol and dried softly by a flow of N_2. The schematic preparation process of the Ag nanostructures on AlF is shown in Fig. 1(a).

The morphologies of as-synthesized shape-diversified Ag nanostructures on AlF were obtained by a field emission scanning electron microscope (FESEM, S-4800 from HITACHI). Fig. 2 and Fig. 3 show the morphology characters of shape-diversified silver nanostructures obtained at room temperature for different growth times when the $AgNO_3$ concentration was 0.3 M on the top view. Fig. 2 (a)–(f) are the FESEM images with low magnification of the silver nanostructures for 1 h, 2 h, 5 h, 8 h, 16 h, 24 h growth times, respectively, which shows that coverage ratio of silver nanostructures increases with growth time. Fig. 3 (a)–(f) are the magnified images of Fig. 2 (a)–(f) respectively, from which we can observe that the fabricated silver nanostructure clusters are composed of silver nanostructures whose size increases with the growth time. Between the silver nanostructures there are many horns and thin gaps. The sizes of silver nanostructures and the roughened clusters increase with growth time. Fig.2 (g)–(l) and Fig.3 (g)-(l) are size distribution histograms of silver clusters and nanotips/nanoplates obtained by different growth times, respectively. When the growth time are 1 h and 2 h (Fig. 2(a) and (b)), the silver clusters are quite like coral comprised of silver nanostructures. Combining with the side view picture (Fig. 4(a) and Fig. 4(b)), we can see that the silver clusters consist of many thin plates which shows as many nanotips on the top view. When the growth time is 1 h, the silver clusters with a mean size of 650 nm comprised of nanoplates whose nanotips average diameter is about 35 nm are obtained. As growth time increases, the nanostructures and cluster growth up. When the growth time is 2 h, the silver clusters become to 1.04 μm comprised of nanoplates whose nanotips average diameter is about 42 nm. As time increases, the shape of silver nanostructure changed from thin nanoplates with nanotips to thicker nanoplates. When the growth time is 5 h, the silver clusters become to 2.5 μm comprised of nanoplates with about 266 nm thickness. With the growth time increasing, the nanoplates become to nanoprisms with thickness and width. The thicknesses of the silver nanostructures are with mean

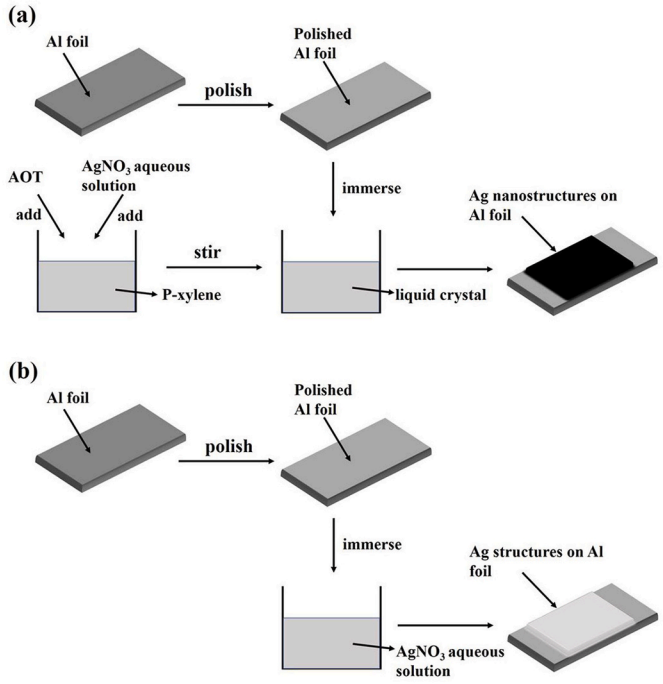

Fig. 1. The schematic preparation process of the Ag–Al substrates. (a) is the preparation process of Ag nanostructures on AlF with micellar template and (b) is the preparation process of Ag structures on AlF without micellar template.

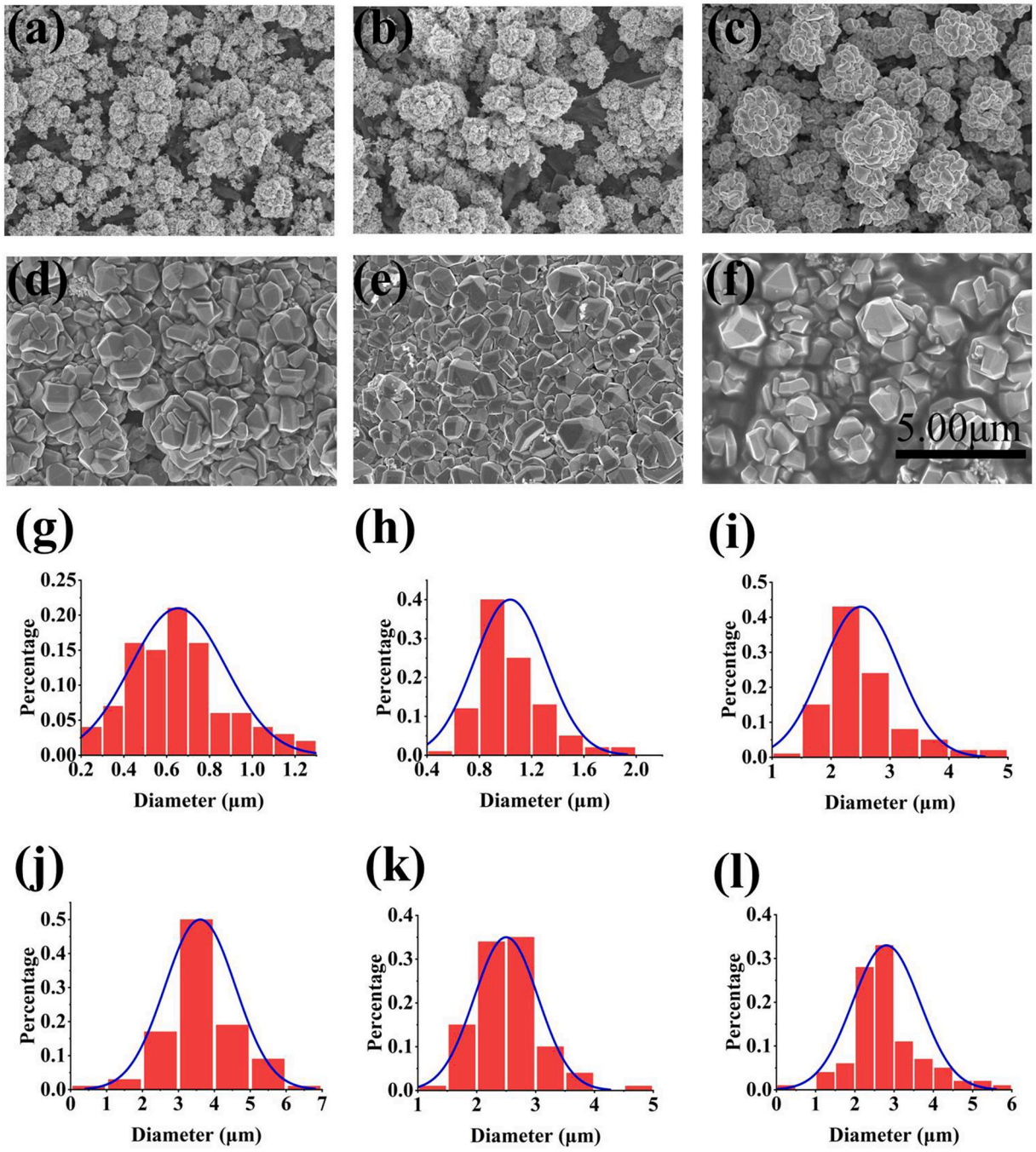

Fig. 2. The FESEM images on the top view with low magnification (a–f) and corresponding Ag clusters' size distribution of shape-diversified silver nanostructures obtained in micellar template at room temperature for different growth times (g)–(l). (a)–(f) are the FESEM images of the silver nanostructures for 1 h, 2 h, 5 h, 8 h, 16 h, 24 h growth times, respectively, which shows that coverage ratio of silver nanostructures increases with growth time.

sizes of 320 nm, 357 nm and 422 nm for 8 h, 16 h and 24 h. The cluster average diameter become to 3.61 μm for 8 h. When the growth time increases to 16 h, dense silver membranous obtained, on the top of which, there are bulges owing to the clusters. The average diameters of the bulges are about 2.5 μm and 2.8 μm for 16 h and 24 h, respectively. The relationship between silver clusters size and the growth time is shown in Fig. 4(g). Fig. 4(h) shows the relationship between silver nanostructure size and the growth time.

Fig. 4 (a-f) are side views of the Ag nanostructures on AlFs obtained by 1 h, 2 h, 5 h, 8 h, 16 h and 24 h, respectively. The relationship between Ag nanostructures height on AlFs and the growth time is shown in Fig. 4(i). From the pictures, we can see that the height of the Ag nanostructures on AlFs increases with growth time. The height of the silver nanostructures are about 1 μm, 1.4 μm, 1.8 μm, 3.5 μm, 4.2 μm and 5 μm for 1 h, 2 h, 5 h, 8 h, 16 h and 24 h, respectively.

In order to study the role of the micellar template played in the silver nanostructure growth process, we designed a reference group in which the silver structures were obtained by galvanic replacement reaction between Al and silver ion without micellar template. The other operation and experimental environment were the same as the experimental group mentioned above. Fig. 1(b) shows the schematic preparation process.

The pictures of the reference group Ag structures on AlFs obtained without micellar template are shown in Fig. S1 and Fig. S2. Fig. S1

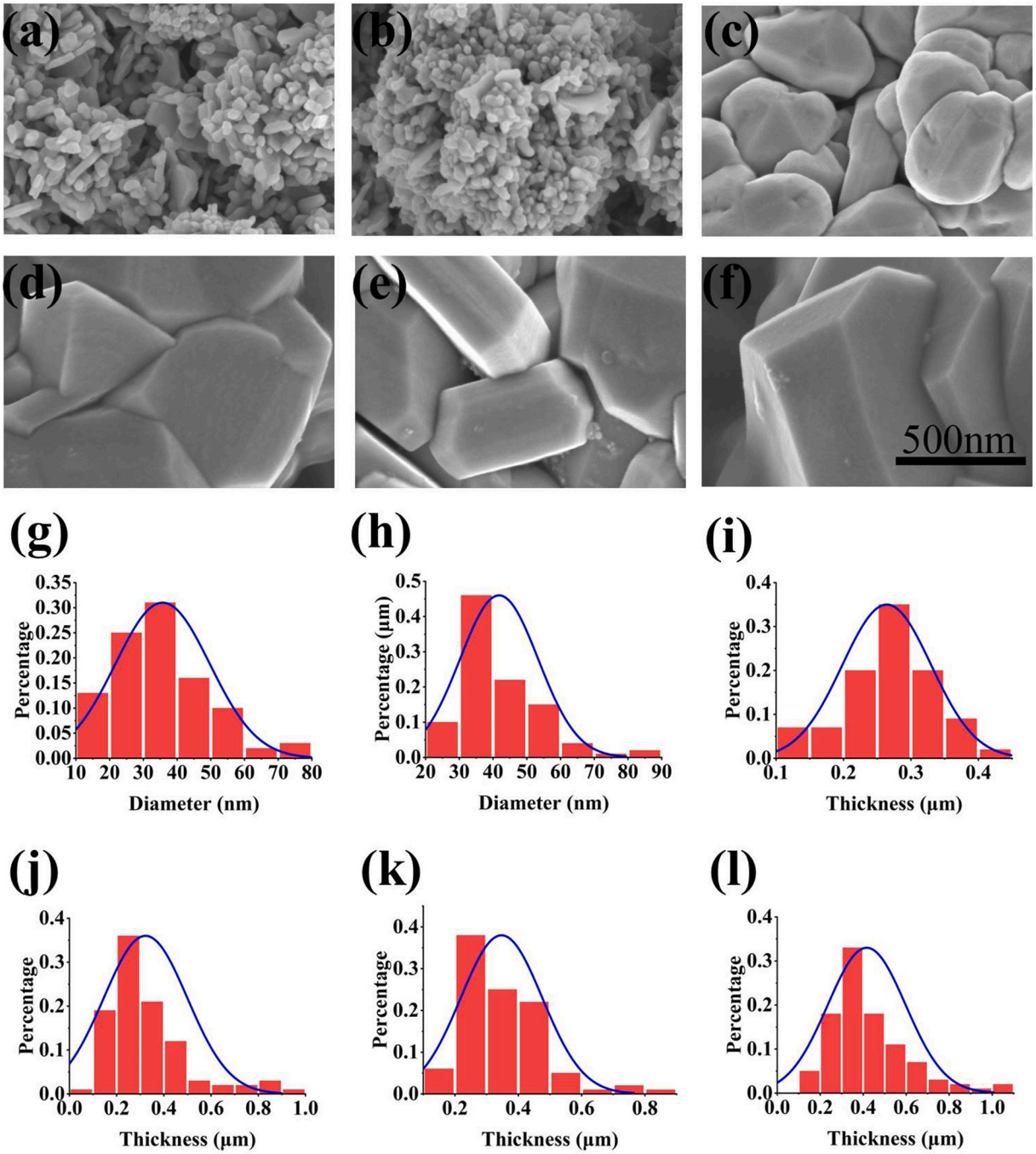

Fig. 3. The FESEM images on the top view with high magnification (a–f) and corresponding Ag nanotips/nanoplates size distribution of shape-diversified silver nanostructures obtained in micellar template at room temperature for different growth times (g–l). (g–h) are nanotip diameter distributions of shape-diversified silver nanostructures. (i–l) are nanoplate thickness distributions of shape-diversified silver nanostructures. (a)–(f) are the magnified images of Fig. 2 (a)–(f), respectively.

represents that macroscopical particles in silver which are so easy to fall off were obtained. From Fig. S2, we can see that dense silver membranous with some large particles have been formed when the growth time is only 1h. The particles grow up with the growth time increasing. When growth time is larger than 16 h (Fig. S1 (e) and (f)), the macroscopical particles can early come off the AlF.

2.2.2. Preparation of Ag nanostructures on ITO glass substrate

The flowerlike silver nanostructures on ITO glass substrate were fabricated in the micellar template by electrodeposition as we reported [38]. Hereafter a brief description is given. The micellar template was prepared as the method mentioned in part 2.2.1. In the electrodeposition process, ITO glass (the cathode, 15 × 30 mm^2) and silver foil (the anode) were mounted to form a cell whose cell gap was 0.7 mm. The ITO glass was used for collecting the flowerlike silver nanostructures whose surface was required to very clean and smooth. Between the anode and cathode, a 3.0V DC voltage was applied at room temperature (~22 °C). The deposition time was 5 h. When the deposition process was finished, the negative electrode ITO glass with silver nanostructures was washed gently by ethanol and dried softly by a flow of N_2.

2.3. Optical properties

Absorption and scattering spectra of the substrates were observed by

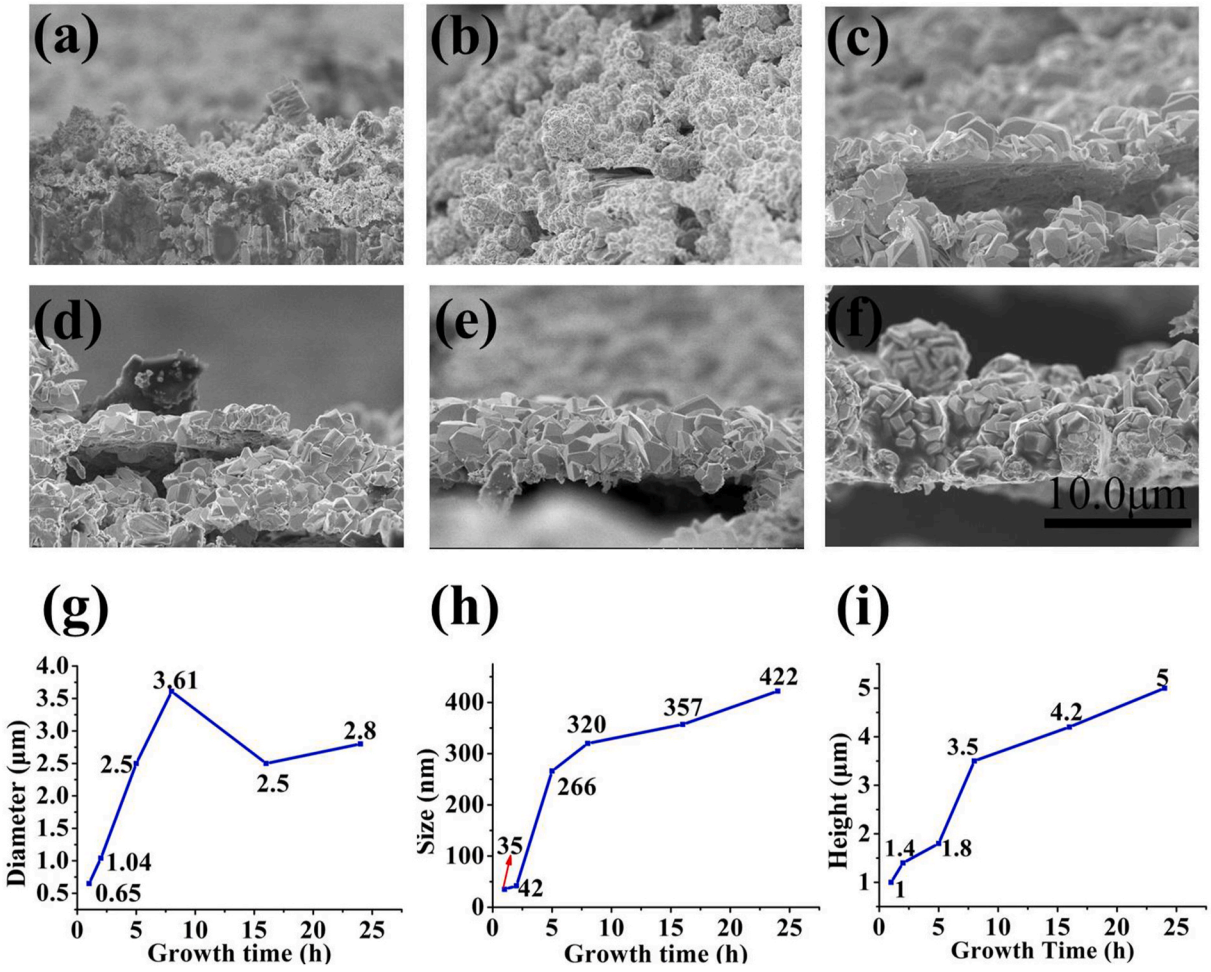

Fig. 4. (a–f) are the FESEM images on the side view of the shape-diversified silver nanostructures on AlFs obtained by 1 h, 2 h, 5 h, 8 h, 16 h and 24 h, respectively. (g–i) are relationships between silver clusters size, silver nanostructures size, silver nanostructures height and the growth time, respectively.

the Perkin Elmer Lambda 950 spectrometer with an integrating sphere.

2.4. Raman measurement

Three Raman probes of 4-MBA, melamine and R6G were chosen. The Ag nanostructures on AlF substrates obtained by grown for different times (obtained with and without micellar template), the Ag nanostructures on ITO glass substrate, and polished AlF substrate were immerged in 50 μM aqueous solution of 4-MBA, R6G and melamine overnight. Then, the nanostructures were washed with deionized water. The Ag nanostructures on ITO glass, Ag structures on AlF substrates obtained without micellar template and polished AlF substrates as reference groups.

The Raman spectra were obtained by an Ocean Optics QE 65 Pro spectrometer and Beijing Htnova CR2000 handed Raman spectrometer. For Ocean Optics QE 65 Pro spectrometer, an InPhotonics 785 nm Raman fiber optics probe with a 200 μm collection fiber and a 105 μm excitation fiber was used for collection and excitation. The numerical aperture was 0.22. 1 s accumulation times was chosen for the samples. The limit of detection for R6G was obtained by Beijing Htnova CR2000 handed Raman spectrometer with 785 nm excitation. 1.2 s accumulation times was chosen for the samples. The power and power density on the sample were 50 mW and $7 \times 10^6 mW/cm^2$, respectively. The time stability of the SERS signal is good as at least a week. The experiments were carried out at room temperature.

3. Results and discussion

3.1. Morphology characterization

Comparing to the macroscopical silver structures on AlFs obtained by galvanic replacement reaction without micellar template, in the fabrication of nanostructure substrates process, the micellar template plays an important role. In the galvanic replacement reaction process, the micellar template controls the formation of nanostructures. The synergistic soft template mechanism [39,40] which refers to both the cooperative effect of the micellar template and the self-assembly of Ag, is supposed to the growth mechanism of such silver nanostructures in micellar template. The AOT, whose molecular structure contains two hydrophobic chains and a hydrophilic head, is a type of amphiphilic molecule, as Fig. 5(a) shows. When the AOT, p-xylene and water are mixed together, firstly, the microphase separation process starts. In this process, micelles with water inside and the hydrophobic tails outside in the p-xylene are formed owing to the hydrophilic heads of the amphiphilic molecule aggregate. When the phase equilibrium is achieved, in the micellar template, there are many water pores surrounded by p-xylene microphase-separated nanostructures [41], as Fig. 5(b) shows. The Ag ions are capsulized in the water pores. The initial nucleation of silver takes place in such pores as Fig. 5(c) illustrates. As the galvanic replacement reaction proceeds ($Al + 3Ag^{+} \rightarrow Al^{3+} + 3Ag$), the aggregated silver nanostructures break the micellar phase template and become shape-diversified nanostructures due to the self-assembly effect of Ag, as shown in Fig. 5(d). The micell acts as a soft template. Because there is no

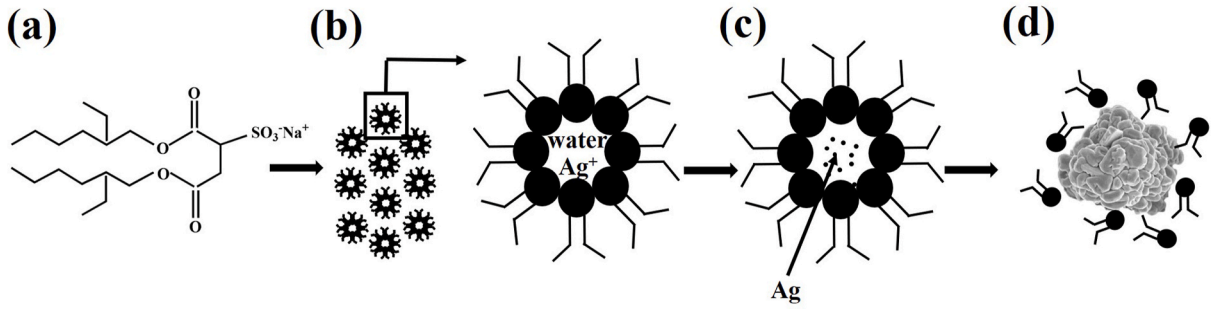

Fig. 5. The schematic illustration for the growth process of silver nanostructures on Al foil with micellar template. (a) The molecular structure of AOT ($C_{20}H_{37}NaO_7S$). The molecule contains two hydrophobic chains and a hydrophilic head. (b) The microphase-separated nanostructure of the template. (c) The initial silver dots deposited at the beginning of the process. (d) The aggregated silver structures break the micellar template and become shape-diversified silver nanostructures as the galvanic deposition process continues.

voltage to control the assignment of the micelles, the nanostructures formed are chaotic and stacked.

3.2. Absorption and scattering properties

Both Ag and Al show particular LSPR properties dependent on the morphology and structures [42]. It is well known that the position and intensity of the LSPR bands depend on the size, shape, aspect ratio, and mutual coupling of silver nanostructures and nanoclusters [43]. As we know, scattering and absorption will occur when the beam goes through the scattering body. The extinction is equal to the scattering and the absorption which is usually used to characterize the localized surface plasmon resonance (LSPR) properties and can be calculated by 1-T (T stands for transmission) [33,44,45]. In our experiment, we tried to characterize the LSPR properties of the samples by measuring extinction. However, the transmitted light intensity is 0 at each wavelength from 400 nm to 800 nm, which means the extinction ratios of samples at each wavelength from 400 nm to 800 nm are 100%. The coupling between the localized surface plasmon of nanostructure and the delocalized surface plasmon polariton from Al film occurred in the range of nm [46]. So, we need to measure the extinction properties of silver nanostructures and Al in the thickness range of nm around them which is impossible for the substrate in current state. In order to explore the effect of silver nanostructures with different shapes and morphologies on the optical properties of the samples and the different optical properties between the samples obtained with and without micellar template, we measured the scattering and absorption properties of the samples.

Fig. 6(a) and Fig. 6(b) show absorption spectra and scattering spectra of the as-prepared Ag nanostructures on AlF samples. Fig. 6(c) and (d) are relationships between absorption/scattering intensity ratios and growth time at 785 nm of silver nanostructures on Al foils obtained with micellar template. Overall through, the absorption spectrum tends to be flat, which can be explained by the fact that the sample consists of Ag nanostructures and the AlF whose thickness is as thick as 10 μm. As the growth time increases, the absorption intensity of the substrates first increases and then decreases. Combined with the FESEM images, the change is due to the size of the nanostructures. From the FESEM pictures, the sizes of nanostructures on the substrates obtained for 1 h, 2 h, 5 h, 8 h, 16 h and 24 h are 35 nm, 42 nm, 266 nm, 320 nm, 357 nm, 422 nm, respectively. As the nanostructure grow up, scattering of the sample first decreases and then increases (Fig. 6(b)), which changes the scattering character of the Ag nanostructures which increases as the

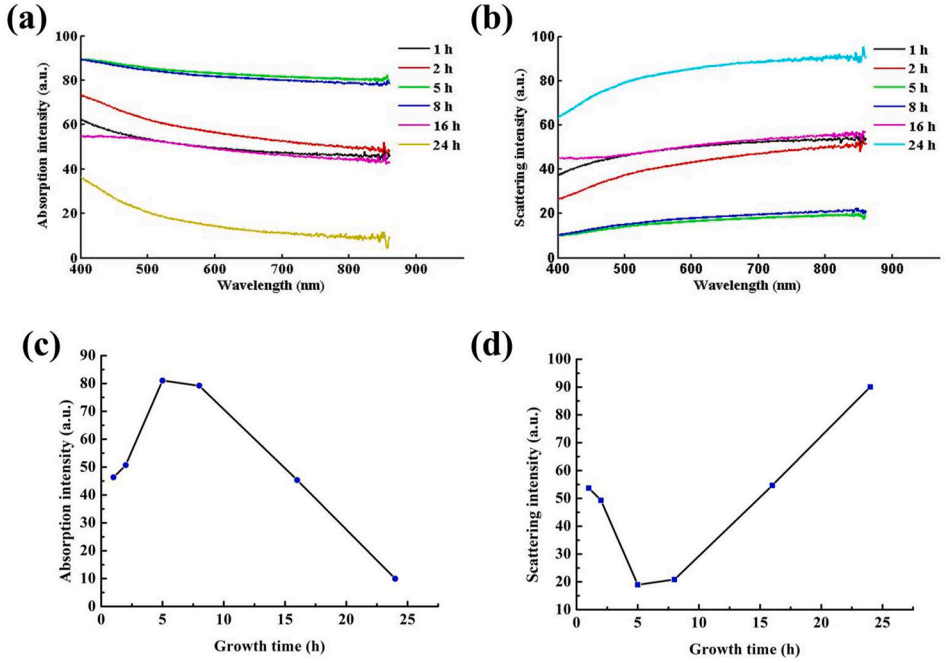

Fig. 6. The absorption spectra (a), scattering spectra (b), relationships between absorption (c)/scattering (d) intensity ratios and growth time at 785 nm of silver nanostructures on Al foils obtained with micellar template.

nanostructure grow up as the literature said [47,48]. The absorption properties of materials grown without micellar template were analyzed. From Fig. S3 we can see that the absorption intensity of the material decreases with the grow time increasing, which represents the sizes of the structures increases with the growth time increasing again.

From the results, we can see shapes and morphologies of silver nanostructures have a certain impact on the optical properties of silver nanostructures on AlF samples. As the literature report [48], the relative scattering intensity increases with the increase of nanostructure size. However, as our measured results, the relative scattering intensity decreases first and then increases with the increase of nanostructure size. This result mainly comes from the plasmon interaction between aluminum substrate and shape-diversified silver nanostructure or between nanostructures. Compared with the materials grown with micellar template, the materials grown without micellar template are different, which illustrates that the micellar template played a key role in refinement of materials.

3.3. Surface enhanced Raman scattering effect

We studied the SERS properties of shape-diversified silver nanostructures on AlF obtained in micellar template with 1 h, 2 h, 5 h, 8 h, 16 h and 24 h growth time comparing with the polished AlF substrate, flowerlike silver nanostructure on ITO glass substrates and silver structures on AlF substrates obtained without micellar template. Three matter of R6G, 4-MBA and melamine were chosen as Raman probes. R6G and 4-MBA are two kinds of common Raman probes which are used widely in various field researches such as cell label, random laser and so on [49]. Melamine is an organic nitrogen-rich chemical, whose rapid detection with trace amounts given to a lot attention owing to its improper added in human food. Molecular structures of the three Raman probes are shown in Fig. S4.

Figs. S5, S6, S7 show the raw SERS spectra of R6G, 4-MBA and melamine on different substrates, respectively. In order to facilitate comparison and observation, these Raman spectra have been smoothed and baseline corrected which are shown in Figs. 7(a) and 8(a), 9(a), respectively. Curves (from top to bottom) represent Raman from shape-diversified silver nanostructures on AlF of 1 h, 2 h, 5 h, 8 h, 16 h and 24 h growth time, flowerlike silver structures on ITO glass substrate and silver structures on AlF which are used as reference curves, respectively. In the experiment, we found that the Raman signal on silver structure AlF obtained without micellar template could not be detected in the experiment condition which shows that the SERS effects of these substrates are weaker compared with substrates mentioned above. We can see that the Raman signals of Raman probes are obviously enhanced by the nanostructure substrates. The intensities of the Raman on shape-diversified silver nanostructure AlFs are much stronger than that on the polished Al substrates and flowerlike silver structures on ITO glass substrate. On the whole, it can be seen that the maximum enhancement effect is achieved by different substrates for different Raman probes. The intensity of SERS signals at different frequencies as a function of the growth time are shown in Figs. 7(b), 8(b) and 9(b). For R6G, the vibrations locating around 777 cm^{-1}、1189 cm^{-1}、1317 cm^{-1}、1604 cm^{-1} and 1656 $cm^{-1}$are enhanced remarkably, as has been reported in the literature [49]. From Fig. 7(b), we can see that the Raman enhanced effect of silver nanostructures on AlF of 8 h is the best. The peak intensity at 777 cm^{-1} obtained by silver nanostructure on AlF of 8 h is 18 times larger than the flowerlike silver nanostructures on ITO glass substrate. The enhancement factor (EF) is estimated as5.8×10^7. For 4-MBA, the vibrations locating around 1082 cm^{-1}、1179 cm^{-1} and 1595 $cm^{-1}$are enhanced remarkably, as has been reported in the literaure [50]. From Fig. 8(b), we can see that different enhancement effects of different vibration are obtained. The best Raman enhanced effect is obtained by silver nanostructures on AlF of 16 h at 1082 cm^{-1} and 1595 cm^{-1}. As at 1179 cm^{-1}, the best is obtained by silver nanostructures on AlF of 5 h. The peak intensity at 1082 cm^{-1} obtained by silver nanostructure on AlF is 236 times larger than the flowerlike silver nanostructures on ITO glass substrate whose EF is estimated as large as 10^9. For melamine, the vibrations locating around 564 cm^{-1}、704 cm^{-1} 、987 $cm^{-1}$and 1232 $cm^{-1}$are enhanced remarkably, as has been reported in the literaure [51]. From Fig. 9(b), we conclude that the best Raman enhanced effect is obtained by silver nanostructures on AlF of 5 h at 704 cm^{-1} and 1232 cm^{-1},while, which is obtained by silver nanostructures on AlF of 2 h at 564 cm^{-1} and 987 cm^{-1}. EF is estimate at 987 cm^{-1} which is as large as 10^6. Detailed processes of EF calculation are shown in supplementary information.

The limit of detection for R6G on shape-diversified silver nanostructure AlF was measured. Fig. 10 (a) shows the SERS spectra of R6G with different concentrations of 10^{-6}M, 10^{-8}M, 10^{-10}M and 10^{-12}M adsorbed on shape-diversified silver nanostructures AlF obtained for 8 h. The intensity of the characteristic R6G peaks decreased as the concentration decreased. The characteristic SERS peak around 613 cm^{-1} is selected for quantification of SERS signal. The corresponding calibration curve between SERS signal intensity at 613 cm^{-1} and the R6G concentration is shown in Fig. 10 (b). A good linear relationship was shown at the given concentration range. The detection limit can reach a low as

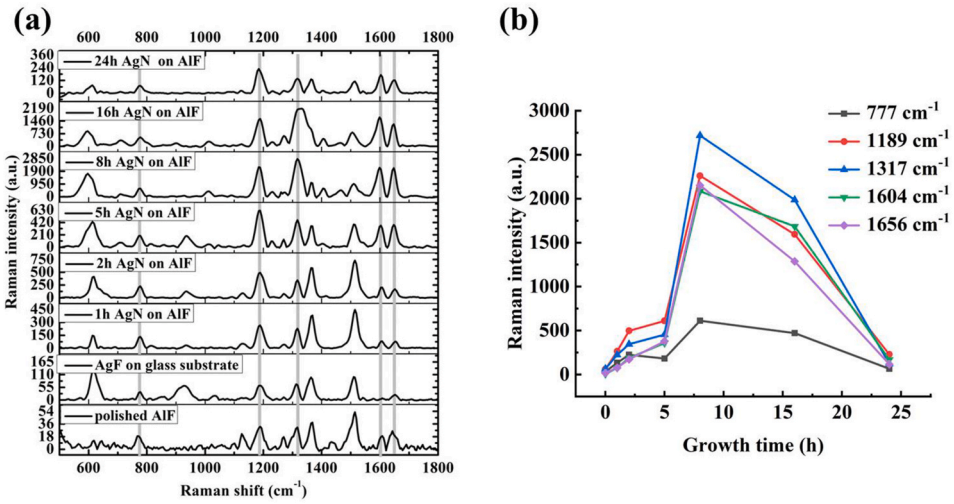

Fig. 7. SERS properties of R6G on different substrates. (a) is smoothed and baseline corrected Raman spectra. AgN on AlF represents Ag nanostructures on AlFs obtained with micellar template. AgF on glass substrate represents flowerlike silver nanostructures on ITO glass substrate obtained with micellar template. (b) is the intensity of SERS signals at different frequencies as a function of the growth time. Flowerlike silver nanostructure substrate is defined as growth time is zero.

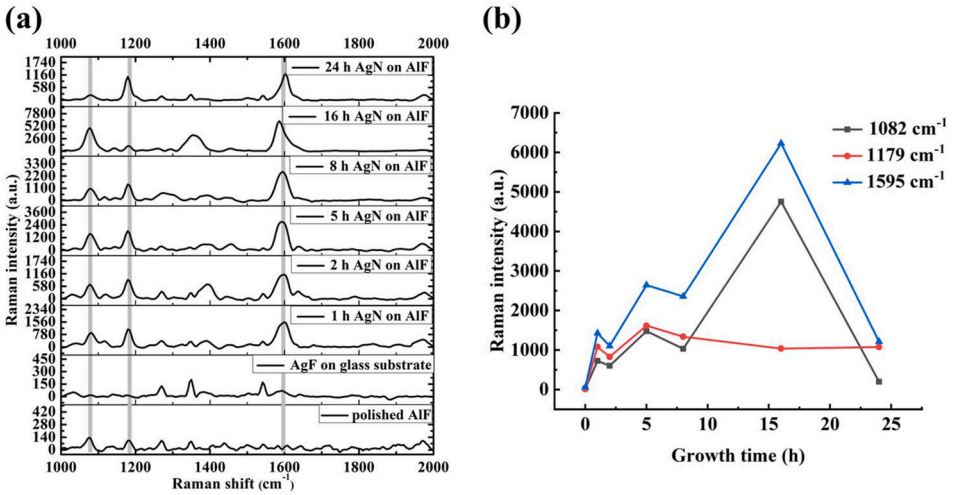

Fig. 8. SERS properties of 4-MBA on different substrates. (a) is smoothed and baseline corrected Raman spectra. AgN on AlF represents Ag nanostructures on AlFs obtained with micellar template. AgF on glass substrate represents flowerlike silver nanostructures on ITO glass substrate obtained with micellar template. (b) is the intensity of SERS signals at different frequencies as a function of the growth time. Flowerlike silver nanostructure substrate is defined as growth time is zero.

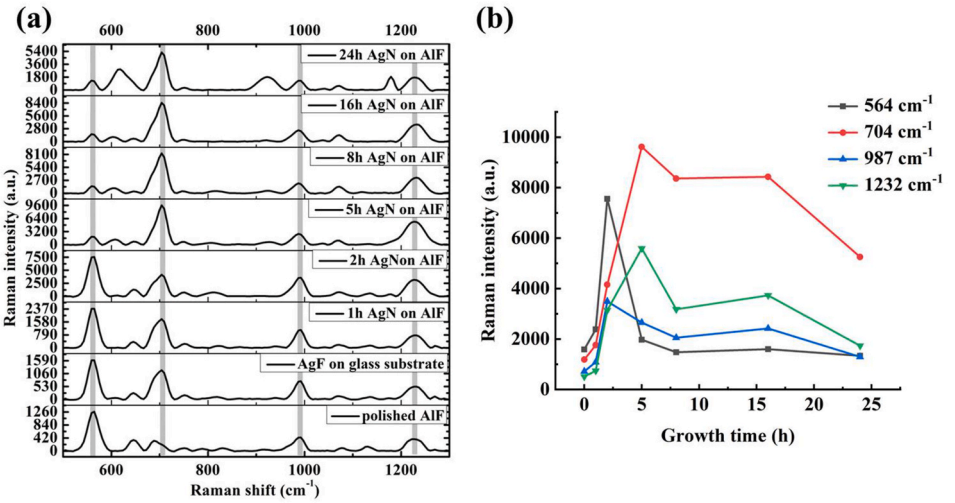

Fig. 9. SERS properties of melamine on different substrates. (a) is smoothed and baseline corrected Raman spectra. AgN on AlF represents Ag nanostructures on AlFs obtained with micellar template. AgF on glass substrate represents flowerlike silver nanostructures on ITO glass substrate obtained with micellar template. (b) is the intensity of SERS signals at different frequencies as a function of the growth time. Flowerlike silver nanostructure substrate is defined as growth time is zero.

10^{-12} M.

From the Raman results, we conclude that the Raman enhancement effect of shape-diversified silver nanostructures on AlF obtained with micellar template is better than the flowerlike silver structure on ITO glass substrates and silver structure on AlF obtained without micellar template. The maximum Raman enhancement factor is 236 times larger than the flowerlike silver nanostructure on ITO glass substrate, which comes up to 10^9 fold. The enhancement effects of the metal nanostructures and the enhancement effects for different probes are size-dependent. And the maximum enhancement effects of different vibrations are different.

According to the general theory, the SERS enhancement for molecules adsorbed on metal nanostructures is attributed to electromagnetic mechanism (EM) and chemical mechanism (CM) [52]. Electromagnetic mechanism is in relation to resonance between the plasmon of the metal surface and the incident ray, in which the morphology, shape and size of the metal nanostructures plays a key role. Chemical mechanism is divided to three mechanism: charge transfer (CT) mechanism where the incident beam is resonant with an excitation from metal to the adsorbate, molecular resonance mechanism related to resonance between the incident beam with a molecular excitation, and nonresonant interactions between the adsorbate and the surface (CHEM), which are related to the adsorbate and metal [52]. In most cases, it is accepted that EM mechanism is the strongest enhancement stem. In our study, enhancement of different substrates for the same Raman probe is different stemming mainly from EM mechanism and partly from CM. The morphologies of silver nanostructures on different substrate are different which lead to different Raman enhancement effects. Combing with the SEM images, plenty of "hot spots" on the metal nanostructures leads to the strong Raman enhancement effect. Besides, the chemical enhancement is also size-dependent [53], which plays a part role in the different enhancement by different substrates for the same Raman probe. The maximum enhancement effects of different vibrations of Raman probes are different. Different vibrations of same Raman probe or different Raman probes undergo different CM mechanism which leads to different Raman enhancement effect. Considering the experiment results and the theoretical analysis, in order to obtain the best Raman enhancement effect, we should chose appropriate SERS substrate

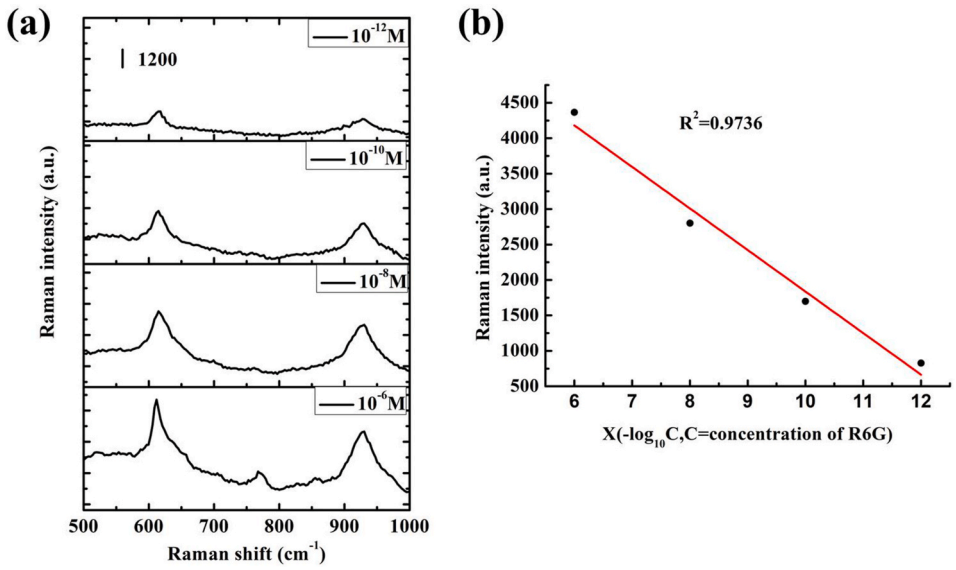

Fig. 10. (a) SERS spectra of R6G with different concentrations adsorbed on shape-diversified silver nanostructures AlF obtained for 8 h in the range near characteristic vibration. (b) The intensity of SERS signals at 613 cm^{-1} as a function of the logarithm of R6G concentration.

according to the actual condition. Shape-diversified silver nanostructures on Al foil controllably fabricated in this study are good candidates for potential applications in SERS field.

4. Conclusion

In this work, we have demonstrated the highly effective surface enhanced Raman scattering substrate with shape-diversified silver nanostructures on AlF fabricated by galvanic replacement reaction in micellar template. Shape-diversified silver nanostructures with different morphologies on AlF were synthesized and investigated by experiments. The enhanced Raman effect of the substrates for R6G, 4-MBA and melamine were studied which shows that the SERS effect is related to the Raman probe and different vibrational modes. The best EF is about 10^9 which is 236 times larger than the flowerlike silver nanostructures on ITO glass. The reasons that surface morphology and shape of the silver nanoparticles play significant roles in enhancing SERS were discussed by analyzing the results of optical spectra and SEM images according to electromagnetic mechanism (EM) and chemical mechanism. Experimental results show that the morphology and shape of shape-diversified nanostructures on AlF plays an important role in SERS. Considering the ultra-sensitive SERS effect together with the simple fabrication method and low cost property, the shape-diversified silver nanostructures on AlFs fabricated by galvanic replacement reaction in micellar template are good candidates for potential applications in SERS field.

CRediT authorship contribution statement

Ying Zhang: Methodology, Visualization, Investigation, Writing – original draft. **Lishuang Yao:** Resources, Investigation. **Lixiang Liu:** Data curation. **Zenghui Peng:** Resources, Methodology. **Zepeng Li:** Resources, Investigation, Validation. **Hao Wang:** Data curation. **Qingjun Zhou:** Investigation, Supervision. **Tong Wei:** Resources, Supervision. **Yanrui Guo:** Resources, Data curation. **Xiong Yang:** Resources. **Li Xuan:** Resources, Supervision.

Declaration of competing interest

The authors declare that they have no known competing financial interests or personal relationships that could have appeared to influence the work reported in this paper.

Acknowledgments

This work is supported by the Fundamental Research Funds for the Central Universities of Civil Aviation University of China (Grant No. 3122019150).

Appendix A. Supplementary data

Supplementary data to this article can be found online at https://doi.org/10.1016/j.optmat.2021.111629.

References

[1] S. Lin, W.L.J. Hasi, X. Lin, S.Q.G.W. Han, X. Lou, F. Yang, D.Y. Lin, Z.W. Lu, Rapid and sensitive SERS method for determination of Rhodamine B in chili powder with paper-based substrates, Anal. Methods 7 (2015) 5289, https://doi.org/10.1039/C5AY00028A.
[2] H. Tang, G. Meng, Z. Li, C. Zhu, Z. Huang, Z. Wang, F. Li, Hexagonally arranged arrays of urchin-like Ag hemispheres decorated with Ag nanoparticles for surface-enhanced Raman scattering substrates, Nano Res 8 (2015) 2261–2270, https://doi.org/10.1007/s12274-015-0737-7.
[3] Z. Zuo, Z. Kai, L. Ning, G. Cui, J. Qu, C. Ying, J. Wang, S. Yi, D. Xu, X. Yu, Highly sensitive surface enhanced Raman scattering substrates based on Ag decorated Si nanocone arrays and their application in trace dimethyl phthalate detection, Appl. Surf. Sci. 325 (2015) 45–51, https://doi.org/10.1016/j.apsusc.2014.10.181.
[4] L. Mandrile, A.M. Giovannozzi, F. Durbiano, G. Martra, A.M. Rossi, Rapid and sensitive detection of pyrimethanil residues on pome fruits by Surface Enhanced Raman Scattering, Food Chem. 244 (2018) 16–24, https://doi.org/10.1016/j.foodchem.2017.10.003.
[5] J. Zhu, M.J. Liu, J.J. Li, X. Li, J.W. Zhao, Multi-branched gold nanostars with fractal structure for SERS detection of the pesticide thiram, Spectrochim. Acta 189 (2017) 586, https://doi.org/10.1016/j.saa.2017.08.074.
[6] J. Ashley, K. Wu, M.F. Hansen, M.S. Schmidt, Y. Sun, Quantitative detection of trace level cloxacillin in food samples using magnetic MIP extraction and SERS nanopillars, Anal. Chem. 89 (2017) 11484–11490, https://doi.org/10.1021/acs.analchem.7b02725.
[7] C. Muehlethaler, M. Leona, J.R. Lombardi, Review of surface enhanced Raman scattering applications in forensic science, Anal. Chem. 88 (2016) 152–169, https://doi.org/10.1021/acs.analchem.5b04131.
[8] T. Jiang, X. Wang, J. Zhou, H. Jin, The construction of silver aggregate with inbuilt Raman molecule and gold nanowire forest in SERS-based immunoassay for cancer biomarker detection, Sensor. Actuator. B Chem. 258 (2018) 105–114, https://doi.org/10.1016/j.snb.2017.11.084.
[9] M. Sun, Z. Zhang, P. Wang, Q. Li, F. Ma, H. Xu, Remotely excited Raman optical activity using chiral plasmon propagation in Ag nanowires, Light Sci. Appl. 2 (2013) e112, https://doi.org/10.1038/lsa.2013.68.
[10] M.J. Mulvihill, Y.L. Xing, J. Henzie, P. Yang, Anisotropic etching of silver nanoparticles for plasmonic structures capable of single-particle SERS, J. Am. Chem. Soc. 132 (2010) 268–274, https://doi.org/10.1021/ja906954f.

[11] Y. Huang, Y. Fang, Z. Zhang, L. Zhu, M. Sun, Nanowire-supported plasmonic waveguide for remote excitation of surface-enhanced Raman scattering, Light Sci. Appl. 3 (2014) e199, https://doi.org/10.1038/lsa.2014.80.
[12] Z. Zhu, B. Bai, O. You, Q. Li, S. Fan, Fano-resonance boosted cascaded field enhancement in a plasmonic nanoparticle-in-cavity nanoantenna array and its SERS application, Light Sci. Appl. 4 (2015) e296, https://doi.org/10.1038/lsa.2015.69.
[13] L. Hu, Y.J. Liu, Y. Han, P. Chen, C. Zhang, C. Li, Z. Lu, D. Luo, S. Jiang, Graphene oxide-decorated silver dendrites for high-performance surface-enhanced Raman scattering applications, J. Mater. Chem. C 5 (2017) 3908–3915, https://doi.org/10.1039/C7TC00381A.
[14] H. Zhao, Y. Guo, S. Zhu, Y. Song, J. Jin, W. Ji, W. Song, B. Zhao, B. Yang, Y. Ozaki, Facile synthesis of silver nanoparticles/carbon dots for a charge transfer study and peroxidase-like catalytic monitoring by surface-enhanced Raman scattering, Appl. Surf. Sci. 410 (2017) 42–50, https://doi.org/10.1016/j.apsusc.2017.03.049.
[15] X. Fu, T. Jiang, Z. Qian, H. Yin, Charge-transfer contributions in surface-enhanced Raman scattering from Ag, Ag_2S and Ag_2Se substrates, J. Raman Spectrosc. 43 (2012) 1191–1195, https://doi.org/10.1002/jrs.4033.
[16] M.D. Porter, R.J. Lipert, L.M. Siperko, G. Wang, R. Narayanan, SERS as a bioassay platform: fundamentals, design, and applications, Chem. Soc. Rev. 37 (2008), https://doi.org/10.1039/B708461G, 1001-1000.
[17] J.A. Creighton, C.G. Blatchford, M.G. Albrecht, Plasma resonance enhancement of Raman scattering by pyridine adsorbed on silver or gold sol particles of size comparable to the excitation wavelength, J. Chem. Soc., Faraday. Trans. Mol. Chem. Phys. 75 (1979) 790–798, https://doi.org/10.1039/F29797500790.
[18] M. Zhang, A. Zhao, H. Guo, D. Wang, Z. Gan, H. Sun, D. Li, M. Li, Green synthesis of rosettelike silver nanocrystals with textured surface topography and highly efficient SERS performances, CrystEngComm 13 (2011) 5709, https://doi.org/10.1039/C1CE05105A.
[19] Y. Nakabayashi, H. Sakai, R. Suzuki, S. Yamada, Formation of silver particles for SERS spectroscopy by mist chemical vapor deposition method, Jap. J. Appl. Phys. 58 (2019) 120908, https://doi.org/10.7567/1347-4065/ab5482.
[20] X. Liang, B. Liang, Z. Pan, X. Lang, Y. Zhang, G. Wang, P. Yin, L. Guo, Tuning plasmonic and chemical enhancement for SERS detection on graphene-based Au hybrids, Nanoscale 7 (2015) 20188–20196, https://doi.org/10.1039/C5NR06010A.
[21] J. Fang, Y. Yi, B. Ding, X. Song, A route to increase the enhancement factor of surface enhanced Raman scattering (SERS) via a high density Ag flower-like pattern, Appl. Phys. Lett. 92 (2008), https://doi.org/10.1063/1.2895639, 131115.
[22] Y.C. Yang, T.K. Huang, Y.L. Chen, J.Y. Mevellec, S. Lefrant, C.Y. Lee, H.T. Chiu, Electrochemical growth of gold nanostructures for surface-enhanced Raman scattering, J. Phys. Chem. C 115 (2011) 1932–1939, https://doi.org/10.1021/jp1073544.
[23] J.C. Hulteen, D.A. Treichel, M.T. Smith, M.L. Duval, T.R. Jensen, R.P. Van Duyne, Nanosphere lithography: size-tunable silver nanoparticle and surface cluster arrays, J. Phys. Chem. B 103 (1999) 3854–3863, https://doi.org/10.1021/jp9904771.
[24] E.C.L. Ru, P.G. Etchegoin, J. Grand, N. Félidj, J. Aubard, G. Lévi, A. Hohenau, J. R. Krenn, Surface enhanced Raman spectroscopy on nanolithography-prepared substrates, Curr. Appl. Phys. 8 (2008) 467–470, https://doi.org/10.1016/j.cap.2007.10.073.
[25] S. Nie, S.R. Emory, Probing single molecules and single nanoparticles by surface-enhanced Raman scattering, Science 275 (1997) 1102–1106, https://doi.org/10.1126/science.275.5303.1102.
[26] M. Luis Liz-Marzán, Tailoring surface plasmons through the morphology and assembly of metal nanoparticles, Langmuir Acs J. Surf. Col. 22 (2006) 32–41, https://doi.org/10.1021/la0513353.
[27] X. Dong, X. Ji, J. Jing, M. Li, J. Li, W. Yang, Synthesis of triangular silver nanoprisms by stepwise reduction of sodium borohydride and trisodium citrate, J. Phys. Chem. C 114 (2010) 2070–2074, https://doi.org/10.1021/jp909964k.
[28] B. Xue, D. Wang, J. Zuo, X.G. Kong, Y.L. Zhang, X.M. Liu, L.P. Tu, Y.L. Chang, C. X. Li, F. Wu, Towards high quality triangular silver nanoprisms: improved synthesis, six-tip based hot spots and ultra-high local surface plasmon resonance sensitivity, Nanoscale 7 (2015), https://doi.org/10.1039/C4NR06901C.
[29] P.K. Jain, W. Huang, M.A. El-Sayed, On the universal scaling behavior of the distance decay of plasmon coupling in metal nanoparticle pairs: a plasmon ruler equation, Nano Lett. 7 (2007) 2080–2088, https://doi.org/10.1021/nl071008a.
[30] F. Zhang, Enhancement of Raman scattering by field superposition of rough submicrometer silver particles, Appl. Phys. Lett. 100 (2012) 1–4, https://doi.org/10.1063/1.4705083.
[31] M. Zhang, A. Zhao, H. Sun, H. Guo, D. Wang, D. Li, Z. Gan, W. Tao, Rapid, large-scale, sonochemical synthesis of 3D nanotextured silver microflowers as highly efficient SERS substrates, J. Mater. Chem. 21 (2011) 18817, https://doi.org/10.1039/C1JM12831K.
[32] A. Gutés, C. Carraro, R. Maboudian, Silver dendrites from galvanic displacement on commercial aluminum foil as an effective SERS substrate, J. Am. Chem. Soc. 132 (2010) 1476–1477, https://doi.org/10.1021/ja909806t.
[33] O. Péron, E. Rinnert, M. Lehaitre, P. Crassous, C. Compere, Detection of polycyclic aromatic hydrocarbon (PAH) compounds in artificial sea-water using surface-enhanced Raman scattering (SERS), Talanta 79 (2009) 199–204, https://doi.org/10.1016/j.talanta.2009.03.043.
[34] J. Dong, S. Qu, Z. Zhang, M. Liu, G. Liu, X. Yan, H. Zheng, Surface enhanced fluorescence on three dimensional silver nanostructure substrate, J. Appl. Phys. 111 (2012), https://doi.org/10.1063/1.4709442, 093101-093101.
[35] J. Dong, H. Zheng, X. Yan, Y. Sun, Z. Zhang, Fabrication of flower-like silver nanostructure on the Al substrate for surface enhanced fluorescence, Appl. Phys. Lett. 100 (2012), 051112, https://doi.org/10.1063/1.3681420.
[36] Yeshchenko, A. Oleg, Kozachenko, V. Viktor, Naumenko, P. Antonina, Berezovska, Gold nanoparticle plasmon resonance in near-field coupled Au NPs layer/Al film nanostructure: dependence on metal film thickness, Photonics Nanostruct. 29 (2018) 1–7, https://doi.org/10.1016/j.photonics.2017.12.005.
[37] Z. Mukanova, K. Gudun, Z. Elemessova, L. Khamkhash, R. Bukasov, Detection of paracetamol in water and urea in artificial urine with gold nanoparticle@Al foil cost-efficient SERS substrate, Anal. Sci. 34 (2018) 183–187, https://doi.org/10.2116/analsci.34.183.
[38] Y. Zhang, C. Yang, X. Xiang, P. Zhang, Z. Peng, Z. Cao, Q. Mu, L. Xuan, Highly effective surface-enhanced fluorescence substrates with roughened 3D flowerlike silver nanostructures fabricated in liquid crystalline phase, Appl. Surf. Sci. 401 (2017) 297–305, https://doi.org/10.1016/j.apsusc.2017.01.010.
[39] W.T. Wu, W. Pang, G. Xu, L. Shi, F. Lu, In situ formation of Ag flowerlike and dendritic nanostructures in aqueous solution and hydrolysis of an amphiphilic block copolymer, Nanotechnology 16 (2005) 2048–2051, https://doi.org/10.1088/0957-4484/16/10/011.
[40] Y. Wan Zhao, On the controllable soft-templating approach to mesoporous silicates, Chem. Rev. 107 (2007) 2821–2860, https://doi.org/10.1021/cr068020s.
[41] P. Ekwall, L. Mandell, K. Fontell, Solubilization in micelles and mesophases and the transition from normal to reversed structures, Mol.Crst. Liq. Cryst. 8 (1969) 157–213, https://doi.org/10.1080/15421406908084903.
[42] M. Rycenga, C.M. Cobley, J. Zeng, W. Li, C.H. Moran, Q. Zhang, D. Qin, Y. Xia, Controlling the synthesis and assembly of silver nanostructures for plasmonic applications, Chem. Rev. 111 (2011) 3669–3712, https://doi.org/10.1021/cr100275d.
[43] T. Huang, F. Meng, L. Qi, Controlled synthesis of dendritic gold nanostructures assisted by supramolecular complexes of surfactant with cyclodextrin, Langmuir 26 (2010) 7582–7589, https://doi.org/10.1021/la904393n.
[44] H. Wang, N. Halas, Mesoscopic Au “meatbal” particles, Adv. Mater. 20 (2008) 820–825, https://doi.org/10.1002/adma.200701293.
[45] E. Petryayeva, U.J. Krull, Localized surface plasmon resonance: nanostructures, bioassays and biosensing—a review, Anal. Chim. Acta 706 (2011) 8–24, https://doi.org/10.1016/j.aca.2011.08.020.
[46] Ross, Michael, B. Schatz, C. George, Radiative effects in plasmonic aluminum and silver nanospheres and nanorods, J. Phys. D Appl. Phys. 48 (2015) 184004, https://doi.org/10.1088/0022-3727/48/18/184004.
[47] P.K. Jain, K.S. Lee, I.H. El-Sayed, M.A. El-Sayed, Calculated absorption and scattering properties of gold nanoparticles of different size, shape, and composition: applications in biological imaging and biomedicine, J. Phys. Chem. B 110 (2006) 7238–7248, https://doi.org/10.1021/jp057170o.
[48] D.D. Evanoff, G. Chumanov, Synthesis and optical properties of silver nanoparticles and arrays, ChemPhysChem 6 (2005), https://doi.org/10.1002/cphc.200500113.
[49] X. Bai, Y. Gao, L. Zheng, Galvanic replacement mediated growth of dendritic gold nanostructures with a three-fold symmetry and their applications to SERS, CrystEngComm 13 (2011) 3562, https://doi.org/10.1039/C1CE05084B.
[50] Yang Libin, Zhang Yu, Ruan Weidong, Zhao Bing, Xu Weiqing, Improved surface-enhanced Raman scattering properties of TiO2 nanoparticles by Zn dopant, J. Raman Spectrosc. 41 (2010) 721–726, https://doi.org/10.1002/jrs.2511.
[51] P. Rajapandiyan, W.L. Tang, J. Yang, Rapid detection of melamine in milk liquid and powder by surface-enhanced Raman scattering substrate array, Food Contr. 56 (2015) 155–160, https://doi.org/10.1016/j.foodcont.2015.03.028.
[52] S.M. Morton, L. Jensen, Understanding the molecule-surface chemical coupling in SERS, J. Am. Chem. Soc. 131 (2009) 4090–4098, https://doi.org/10.1021/ja809143c.
[53] L. Jensen, L.L. Zhao, G.C. Schatz, Size-dependence of the enhanced Raman scattering of pyridine adsorbed on agn (n = 28, 20) clusters, J. Phys. Chem. C 111 (2007) 4756–4764, https://doi.org/10.1021/jp067634y.